Central Pacific El Niño as a precursor to summer drought-breaking rainfall over southeastern Australia

Mandy B. Freund[1,3]

Andrew G. Marshall[2]

Matthew C. Wheeler[3]

Jaclyn N. Brown[4]

[1] CSIRO Oceans and Atmosphere, Aspendale, Victoria, Australia

[2] Bureau of Meteorology, Hobart, Tasmania, Australia

[3] Bureau of Meteorology, Melbourne, Victoria, Australia

[4] CSIRO Oceans and Atmosphere, Hobart, Tasmania, Australia

Monday, 18 January 2021

Corresponding Author: Andrew G. Marshall

Bureau of Meteorology

Hobart, Tasmania, Australia

Andrew.Marshall@bom.gov.au

Key Points:

- The strength of central Pacific (CP) El Niño events has a significant impact on rainfall over southeastern Australia
- Strong CP events cause Australian rainfall deficits during onset but enhanced rainfall over southeastern Australia during the mature phase
- This can be explained by a circulation change over eastern Australia from drier, more westerly flow to moister, more easterly onshore flow

Abstract

Using an extended 120-year record of El Niño events, we distinguish between central Pacific (CP) and eastern Pacific (EP) types to show that the strength of CP events is a factor in the amplitude and sign of the impact on rainfall over southeastern Australia. Both weak and strong CP events cause widespread rainfall deficits in Australia during the onset phase from April to September. However, this relationship reverses over southeastern Australia including the Murray Darling Basin river catchment region for the strongest CP events after October, leading to positive rainfall anomalies during the mature phase of strong CP El Niños. This reversal can be explained by a change in the circulation over eastern Australia from drier, more westerly orientated flow to moister, more easterly onshore flow. These findings may help with seasonal prediction efforts to predict drought-breaking rain such as occurred in early 2020.

Plain Language Summary

El Niño Southern Oscillation (ENSO) events are extremely important for many countries around the world due to their impacts on rainfall. By separating El Niño into central Pacific (CP) and eastern Pacific (EP) events, we show that the strength of a CP event controls the rainfall amount for southeastern Australia. The stronger a CP event is, the drier it is over Australia during the onset phase from April to September. But after October during the mature phase of El Niño, the strongest CP events lead to more rainfall than normal over the southeast Australian river catchment known as the Murry Darling Basin, whereas the weakest CP events lead to less rainfall than normal. This relationship is strongest in January to March around the time that the CP event is fully developed. For the strongest CP events, this can be explained by a change in the

circulation from drier, more westerly flow during the onset phase to moister, more easterly onshore flow during the mature phase. This finding is important for agricultural and water resources planning efforts in the Murry Darling Basin region and may help with seasonal prediction efforts to predict drought-breaking rain such as occurred in early 2020.

1 Introduction

The interannual variability of the tropical Pacific Ocean can have a dominant influence on Australian rainfall, including over the Murray Darling Basin in Australia's southeast [e.g., *Risbey et al.*, 2009], with about 30-60% of Australian annual rainfall explained by variations in the El Niño Southern Oscillation (ENSO) [*Dai and Wigley*, 2000]. The relationship between Australian rainfall and ENSO is widely recognised as being nonlinear, with opposing characteristics between the El Niño (warming) and La Niña (cooling) phases. El Niño events increase the likelihood of dry conditions in many parts of the country including eastern, southeastern and northern Australia [*Nicholls et al.*, 1997]. Given the generally dry Australian climate, rainfall reductions during El Niño events can ultimately lead to severe droughts. In contrast during La Niña, large parts of Australia tend to experience wetter conditions than normal. More frequent extreme high rainfall and generally cooler temperatures during La Niña events increase the risk of flooding [*King et al.*, 2013; *King et al.*, 2014]. While the Australian rainfall response to ENSO is linear for La Niña [*Chung and Power*, 2017; *Cai et al.*, 2010] (i.e. the stronger a La Niña event is, the stronger the rainfall response becomes), the degree of drying during El Niño appears to be unrelated to the strength of the event and therefore, poses high uncertainties and risks for efforts to predict seasonal rainfall. A further consideration is the influence of ENSO on other modes of climate variability, such as the Indian Ocean Dipole (IOD) [e.g. *Saji et al.*, 1999; *Webster et al.*, 1999] and the Southern Annular Mode (SAM) [e.g. *Trenberth*, 1979; *L'Heureux and Thompson*, *2006*], and the rainfall responses to these other modes during ENSO years [e.g. *Risbey et al.*, 2009; *Raut et al.*, 2014]

The overall wetting and drying influences of La Niña and El Niño are widely known and anticipated for Australia but event diversity can diffuse ENSO's impacts. For example, the strong El Niño events in 1982 and 1997 had very different impacts on Australian rainfall [*van Rensch et al.*, 2015]. During the El Niño in 1982, eastern Australia experienced the large rainfall deficits typically expected during El Niño events. However, an El Niño event of similar strength in 1997 resulted in near average rainfall for Australia [*Wang and Hendon*, 2007; *Brown et al.*, 2009], as did the recent El Niño event in 2015 [*van Rensch et al.*, 2019].

Some of these differences have been explained by the complexity of El Niño and its varying spatial characteristics, such that Australian rainfall is likely more sensitive to the spatial distribution of warming across the tropical Pacific Ocean [*Wang and Hendon*, 2007; *Lim and Hendon*, 2015]. El Niño events can be divided into two distinct types, distinguished by their location of warming [*Larkin and Harrison*, 2005; *Ashok and Yamagata*, 2009]. The traditional eastern Pacific (EP) El Niño events exhibit their strongest sea surface warming close to the South American coast, whereas central Pacific (CP) events have their peak warming close to the International Dateline.

Previous analysis of the effects of El Niño in the Australian region has been restricted to a handful of events that occurred after 1979 [*Taschetto and England*, 2009; *Brown et al.*, 2009]. Having only a small number of events to examine will limit the insights that can be made, and thus most research on the non-linearity between Australian rainfall and ENSO to date has focused on the division between La Niña and El Niño without being able to further distinguish between EP and CP event types. In this study we build on the existing efforts by using an extended record of EP and CP events from 1900-2019 [*Freund et al.*, 2019] to present a more differentiated picture of El Niño impacts on Australian rainfall. By focusing on the spatio-temporal differences of EP and CP events and their relationship to Australian rainfall using a long data record, we are able to show that the type of El Niño event is a major factor in determining the teleconnection to Australian rainfall.

2 Data and Methods

We use the Australian Water Availability Project (AWAP) gridded data set of monthly rainfall observations [*Jones et al.*, 2009] to quantify the impacts of El Niño on Australian rainfall. The gridded rainfall dataset encompasses the Australian continent at a horizontal resolution of 0.05° x 0.05° for the period 1900 to 2020. Australian rainfall variability is temporally and spatially highly complex [*Risbey et al.*, 2009]. Therefore, we assess the impact of ENSO on Australian rainfall at both monthly and seasonal timescales. For the seasonal analysis we choose two periods that separate the onset (April-Sept) from the mature (Oct-March) phases of El Niño. These also broadly correspond to the cool and warm seasons for extratropical Australia.

The relationship between Australian rainfall and different types of El Niño is assessed for distinct El Niño events. To maximise the number of El Niño events, we use an extended record of EP and CP El Niño events that starts in 1900 [*Freund et al.*, 2019]. EP El Niño events commence in the years 1902, 1905, 1918, 1930, 1941, 1951, 1957, 1965, 1972, 1976, 1982, 1997 and 2015. CP events commence in the years 1904, 1914, 1923, 1925, 1929, 1939, 1940, 1963, 1968, 1969, 1977, 1979, 1986, 1987, 1991, 1994, 2002, 2004, 2006, 2009, 2014 and 2019. The intensity of El Niño events is derived from sea surface temperature anomalies averaged over the Niño-4 region (Niño-4 index; 160°E to 150°W longitude and 5°N to 5°S latitude) calculated using the HadISST dataset [*Rayner et al.*, 2003]. Atmospheric reanalysis products for mean sea level pressure (MSLP), 850hPa wind and outgoing longwave radiation (OLR) were obtained from the NOAA/CIRES/DOE Twentieth Century Reanalysis version 3 [*Compo et al.*, 2011; *Slivinski et al.*, 2019] for the years 1900 to 2015.

3 Results

The coupled ocean-atmosphere ENSO is depicted in the composites of Figure 1 for each type of El Niño. In the mature phase of CP events there is a zonal tripole pattern in OLR (Figure 1b). This is evidenced by reduced convection (positive OLR anomalies; solid contours) over the Maritime Continent and far western Pacific, enhanced convection (negative OLR anomalies; dashed contours) over the western-central tropical Pacific where the surface warming is most pronounced, and suppressed convection (positive OLR anomalies; solid contours) over the eastern tropical Pacific off the South American coast. EP events on the other hand show a strong zonal SST gradient across the western-central tropical Pacific: reduced SST and convection (positive OLR anomalies) occur west of the Dateline, and pronounced warming and convection (negative OLR anomalies) across the central-eastern tropical Pacific. For both types of El Niño these tropical patterns intensify from the onset phase to the mature phase, and large-scale teleconnection patterns extend into each hemisphere, including over Australia. Here convection is reduced over much of the continent, except over northern Australia during the onset of CP events where OLR anomalies are near-zero (Figure 1a) and over southern Australia during mature EP events where OLR anomalies are negative (increased convection; Figure 1d).

The impact of these convective anomalies on Australian rainfall anomalies is illustrated in Figure 2. Conditions across mainland Australia are anomalously dry for each type of El Niño except in parts of the Top End and Far North Queensland during the onset of CP events (in concert with near-zero convective anomalies in Figure 1a), and in southern parts of Western Australia during mature EP events (in concert with increased convection/cloudiness in Figure 1d), where rainfall increases of up to 30 mm are observed. Otherwise, the greatest impact of CP events on dry conditions in eastern Australia occurs during austral spring (see also *Taschetto and England* [2009]), in contrast to EP events whose greatest impact occurs during the winter months, and hence EP events have a greater impact on rainfall deficits during El Niño onset than CP events.

While Figure 2 shows the average impact on Australian rainfall of each type of El Niño, it says nothing about the relationship of rainfall to the strength of El Niño. Previous research shows a weak relationship of the magnitude of the rainfall impact to El Niño intensity when both types of events are considered together [e.g. *Chung and Power*, 2017], however we show here that if differentiated by the two types of El Niño, the intensity of CP events can have broad significant impacts on rainfall amounts in Australia. Figure 3 shows the correlation between the Niño-4 index and rainfall anomalies. During the onset of CP events (Figure 3a), a strong negative correlation emerges that shows the stronger the El Niño event is, the drier the conditions are in Australia (i.e. the larger the Niño-4 SST anomaly, the more negative the rainfall anomaly). A similar homogenous correlation for EP events cannot be derived (Figure 3c). During the mature phase of El Niño, the correlation for EP events again appears heterogeneous and lacking in statistical significance (Figure 3d), however for CP events (Figure 3b) a strong and significant positive correlation appears across a broad region encompassing the Murray Darling Basin in southeastern Australia. This indicates that from October to March, stronger CP events are associated with higher rainfall totals in southeastern Australia compared with weaker CP events. This conclusion is supported by the scatter plots inset in Figure 3 for CP events, which show a positive correlation between the Niño-4 index and southeast Australian rainfall during the mature phase, in contrast to the negative correlation observed during the onset phase.

To further explore the positive correlation between CP event intensity and southeast Australian rainfall during the mature phase of CP El Niño, we calculate three-month rolling correlations between the Niño-4 index and area-averaged rainfall anomalies in southeast Australia. For this we define a southeast Australian / Murray Darling Basin box region bounded by 138°E to 150°E in longitude and 22°S to 34°S in latitude (illustrated in Figure 3). Figure 4a shows the flip in sign from negative correlation during El Niño onset, to positive correlation after the October to December period (OND). This relationship is strongest from January to March (JFM+) with a significant correlation of around 0.5, highlighting that the mature phase of stronger CP events is associated with larger rainfall totals in the Murray Darling Basin. This is supported by Figure 4b, for which we isolate the strongest (red) and weakest (blue) CP events since 1900 based on the strength of the Niño-4 index, and plot rolling three-month mean rainfall anomalies in southeastern Australia. The three strongest CP events commence in 2009, 1987 and 1994. (2009 is ranked strongest.) The five strongest CP events also include 1940 and 2002, and the seven strongest CP events also include 1968 and 2019. (2019 is ranked seventh strongest.) The three weakest CP events commence in 1914, 1929 and 1963. (1914 is ranked weakest.) The five weakest CP events also include 1904 and 1923, and the seven weakest CP events also include 1979 and 1969. (1969 is ranked seventh weakest.) During the onset phase, rainfall anomalies for the strongest CP events are generally more negative than those for the weakest CP events. After OND however, rainfall anomalies for the strongest CP events become positive and rapidly increase to values of around 40 mm or more by JFM(+), whereas rainfall anomalies for the weakest CP events decrease to around -40 mm or less by this time. Thereafter the rainfall correlation weakens with the decay of El Niño.

The strong CP events in 2009 and 2019 both coincide with the drought-breaking conditions that mark the end of the Millennium drought (1997-2009) [*Freund et al.*, 2017] and the most recent drought (2017/2018-2020). We highlight the most recent CP event in 2019-2020 (grey curve in Figure 4b), which was a strong and persistent event with Niño-4 index values peaking around 0.93 °C in NDJ(+) and remaining greater than 0.50 °C until MAM(+). This event follows a similar evolution to the strongest CP event groupings: Rainfall anomalies in southeastern Australia were strongly negative through 2019 before rapidly increasing to around 20 mm by JFM 2020 (JFM+). We note that the CP event of 2019-2020 was not the only important influence on the dry conditions in 2019, with the IOD also in its positive phase from September 2019 to January 2020 and the SAM in its negative phase from October to December 2019 [*Bureau of Meteorology*, 2020]. These modes of climate variability are also known to have drying influences in southeastern Australia [e.g. *Risbey et al.*, 2009; *Marshall et al.*, 2012]. Thus, the combination of these two modes of variability was also highly favourable for dry conditions there, helping to explain why the rainfall anomaly in the second half of 2019 was considerably less than the average for strong CP events, particularly during OND and NDJ(+). The timing of their demise by December 2019 (negative SAM) and January 2020 (positive IOD) coincides with the sharp increase in rainfall after NDJ(+), and in particular after DJF(+), seen in Figure 4b.

We can understand the contrasting impacts of weak and strong CP events on southeast Australian rainfall by examining broad scale circulation anomalies during the onset and mature phases of El Niño. Figures 4c-f show mean sea level pressure and 850hPa wind patterns for the strongest seven and weakest seven CP events. These are calculated as differences from the CP event climatology, which shows predominantly south to southwesterly flow over southeastern Australia (not shown). The strongest events during JFM(+) (Figure 4d) and the weakest events during ASO (Figure 4e) both produce higher rainfall totals in southeastern Australia (Figure 4b) in concert with anomalous easterly flow. Conversely, the strongest events during ASO (Figure 4c) and the weakest events during JFM(+) (Figure 4f) show drier conditions for southeastern Australia (Figure 4b) in association with more westerly orientated flow. These results point to the preponderance of anomalous onshore flow leading to enhanced southeast Australian rainfall, fed by moisture from an anomalously warm Tasman Sea (Figure 1), while drier air from the west results in reduced rainfall. The underlying MSLP differences indicate higher pressure to the south of the continent driving more onshore flow for the wetter cases (Figures 4d and 4e), in contrast to lower pressure south of the continent driving more westerly flow for the drier cases (Figures 4c and 4f). This result supports previous work that shows wetter air parcel trajectories into southeastern Australia from the east [*Holgate et al.*, 2020], in contrast to drier trajectories from the west, in different El Niño years, often associated with split-flow blocking high pressure systems further south [*Brown et al.*, 2009; *McIntosh et al.*, 2012].

4 Conclusions

This study has shown that rainfall in southeastern Australia, including the Murray Darling Basin, varies linearly with the intensity of CP El Niño events in the onset phase of El Niño. Both EP and CP events are generally associated with large-scale drying across the Australian continent in austral winter and spring, with the greatest impacts on dry conditions in the southeast occurring in winter for EP events and in spring for CP events. However, strong CP events lead to higher rainfall totals in southeastern Australia during the mature phase of El Niño, compared with weak CP events, in association with an enhanced onshore flow from the Tasman Sea. The importance of zonal distributions of tropical Pacific SSTs [*Wang and Hendon*, 2007] and air flow trajectories [*Brown et al.*, 2009] for southeast Australian rainfall have been demonstrated for the strong El Niño events of 1982 (EP), 1997 (EP) and 2002 (CP). We have expanded on this previous work with an extended 120-year record of El Niño events to obtain a more detailed view of the spatial and temporal fingerprints of CP and EP events on Australian rainfall, showing for the first time that the peak of strong CP events tends to be directly followed by enhanced rainfall in the Murray Darling Basin. EP events, on the other hand, do not show a clear relationship between El Niño intensity and Australian rainfall.

The results of this investigation shed some light on the occurrence of major rain events in central and eastern Australia in late summer and early autumn during the mature phase of strong CP events, including 1994-1995, 2009-2010, and 2019-2020 [*National Climate Centre*, 2010; *Bureau of Meteorology*, 2020]. For example, during the most recent 2019-2020 El Niño event, much of the New South Wales coast and southeastern Queensland experienced very much above average rainfall in February 2020 when a persistent surface trough developed along the coast and fed moist, east to northeasterly winds onto the New South Wales coast [*Bureau of Meteorology*, 2020]. Associated with a split-flow blocking high near Tasmania, this extreme rainfall event led to road closures, water rescues, property damage and a nursing home evacuation due to flash flooding. In line with results by *Holgate et al.* [2020], we find that easterly flow is essential for the termination of the drought conditions during strong CP events. Our findings may help with efforts to predict southeast Australian rainfall during the mature phase of strong CP events by providing an improved understanding of the role of onshore flow for driving disruptive rain events such as that observed in February 2020. Given that these events are often associated with split-flow blocking activity, this improved dynamical understanding may be important for diagnosing climate model deficiencies and biases that lead to the underrepresentation and underprediction of blocking activity at subseasonal timescales and beyond [e.g. *McIntosh et al.*, 2008; *Marshall et al.*, 2014]. Identifying the key features that contribute to rainfall patterns thus provides essential knowledge for developing climate prediction systems and improving forecast skill.

This study is an important first step in discerning the impacts of EP and CP El Niño events on Australian rainfall, and is a valuable contribution to recent efforts in assessing relationships between Australian climate and modes of interannual variability using an extended data record [*Gallant et al.*, 2013, *Freund et al.*, 2017]. Follow-on work can include an assessment of air flow and moisture trajectories for strong versus weak CP events, to more fully understand the moisture pathways that lead to extreme rainfall events for the eastern states of Australia [*Brown et al.*, 2009; *McIntosh et al.*, 2012]. Our results point to warming of the Tasman Sea off the east Australian coast (Figure 1) as being important for the provision of moisture to southeastern Australia during the mature phase of strong CP events. The role of local air-sea interaction in modulating ENSO teleconnections to rainfall [*Hendon*, 2003] should therefore be considered in future extensions of this work. The role of other modes of climate variability, such as the IOD and SAM, could also be explored in future work using climate model sensitivity experiments. Finally, the importance of distinguishing CP from EP La Niña events has recently been demonstrated for the coastal climate of Western Australia [*Marshall et al.*, 2015], and thus the sensitivity of Australian rainfall to the different types of La Niña should be examined also.

Our study has pointed to the role of warm ocean temperatures along the coast of Australia during CP events as potentially contributing to drought breaking rainfall. Many studies have shown that this region and the East Australian Current has been one of the faster warmer ocean locations on the planet and is projected to continue to warm. This begs the question of whether such continued warming many contribute to larger rainfall in the future associated with the mature phase of the Central Pacific El Niño. The next phases of this research should explore these hypotheses.

Acknowledgements. This study was supported through funding from CSIRO Agriculture and Food and Oceans and Atmosphere. All data for this paper is properly cited and referred to in the reference list. Support for the AWAP gridded data, available in *Jones et al.* [2009], is provided by CSIRO and the Bureau of Meteorology. The AWAP data used in this paper are openly accessible from https://doi.org/10.4227/166/5a8647d1c23e0, under the CC BY-NC 4.0 International Licence. Support for the HadISST data, available in *Rayner et al*. [2003], is provided by the UK Met Office. The HadISST data used in this paper are openly accessible from https://www.metoffice.gov.uk/hadobs/hadisst, for the purposes of private study and scientific research. Support for the Twentieth Century Reanalysis Project version 3 dataset, available in *Compo et al.* [2011] and *Slivinski et al.* [2019], is provided by the U.S. Department of Energy, Office of Science Biological and Environmental Research (BER), by the National Oceanic and Atmospheric Administration Climate Program Office, and by the NOAA Physical Sciences Laboratory. The Twentieth Century Reanalysis Project version 3 data used in this paper are openly accessible from https://psl.noaa.gov/data/gridded/data.20thC_ReanV3.html.

REFERENCES

Ashok, K, and T. Yamagata (2009), The El Niño with a difference, *Nature, 461*, 481-484.

Brown, J. N., P. C. McIntosh, M. J. Pook, and J. S. Risbey (2009), An Investigation of the Links between ENSO Flavors and Rainfall Processes in Southeastern Australia, *Mon. Wea. Rev., 137,* 3786-3795.

Bureau of Meteorology (2020), extreme heat and fire weather in December 2019 and January 2020, *Special Climate Statement 73*, 1-17. [http://www.bom.gov.au/climate/current/statements/scs73.pdf]

Cai, W., P. van Rensch, T. Cowan, and A. Sullivan (2010), Asymmetry in ENSO teleconnection with regional rainfall, its multidecadal variability, and impact, *J. Clim.*, *23*, 4944-4955.

Chung, C. T. Y., and S. B. Power (2017), The non-linear impact of El Niño, La Niña and the Southern Oscillation on seasonal and regional Australian precipitation, *J. Southern Hem. Earth. Sys. Sci., 67,* 25-45.

Compo, G. P., J. S. Whitaker, P. D. Sardeshmukh, N. Matsui, R. J. Allan, X. Yin, B. E. Gleason, R. S. Vose, G. Rutledge, P. Bessemoulin, S. Brönnimann, M. Brunet, R. I. Crouthamel, A. N. Grant, P. Y. Groisman, P. D. Jones, M. Kruk, A. C. Kruger, G. J. Marshall, M. Maugeri, H. Y.

Mok, Ø. Nordli, T. F. Ross, R. M. Trigo, X. L. Wang, S. D. Woodruff, and S. J. Worley (2011), The Twentieth Century Reanalysis Project, *Quarterly J. Roy. Meteorol. Soc., 137*, 1-28.

Dai, A., and T. M. L. Wigley (2000), Global pattern of ENSO-induced precipitation, *Geophys. Res. Lett., 27,* doi.org/10.1029/1999GL011140.

Freund, M., B. J. Henley, D. J. Karoly, K. J. Allen, and P. J. Baker (2017), Multi-century cool- and warm-season rainfall reconstructions for Australia's major climatic regions, *Clim. Past.*, *13*, 1751-1770, doi:10.5194/cp-13-1751-2017.1

Freund, M. B., B. J. Henley, D. J. Karoly, H. V. McGregor, N. J. Abram, and D. Dommenget (2019), Higher frequency of Central Pacific El Niño events in recent decades relative to past centuries, *Nat. Geoscience, 12*, 450-455.

Gallant, A. J. E., S. J. Phipps, D. J. Karoly, A. B. Mullan, and A. M. Lorrey (2013), Nonstationary Australasian teleconnections and implications for paleoclimate reconstructions, *J. Clim.*, *26*, 8827-8849.

Hendon, H. H. (2003), Indonesian Rainfall Variability: Impacts of ENSO and Local Air–Sea Interaction, *J. Clim., 16*, 1775-1790.

Holgate, C. M., A. I. J. M. V. Dijk, J. P. Evans, and A. J. Pitman (2020), Local and Remote Drivers of Southeast Australian Drought, *Geophys. Res. Lett.*, *47*, e2020GL090238.

Jones, D.A., W. Wang, and R. Fawcett (2009), High-quality spatial climate data-sets for Australia, *Aust. Meteorol. Oceanogr. J.*, *58*, 233-248.

King, A. D., L. V. Alexander, and M. G. Donat (2013), Asymmetry in the response of eastern Australia extreme rainfall to low‐frequency Pacific variability, *Geophys. Res. Lett.*, *40*, 2271-2277.

King, A. D., N. P. Klingaman, L. V. Alexander, M. G. Donat, N. C. Jourdain, P. Maher (2014), Extreme rainfall variability in Australia: patterns, drivers, and predictability, *J. Clim.*, *27*, 6035-6050.

Larkin, N., and D. E. Harrison (2005), On the definition of El Niño and associated seasonal average U.S. weather anomalies, *Geophys. Res. Lett.*, *32*, L13705, doi:10.1029/2005GL022738.

L'Heureux, M. L., and D. W. J. Thompson (2006), Observed relationships between the El Niño–Southern Oscillation and the extratropical zonal-mean circulation, *J. Clim.*, *19*, 276-287.

Lim, E.-P., and H. H. Hendon (2015), Understanding the contrast of Australian springtime rainfall of 1997 and 2002 in the frame of two flavors of El Niño, *J. Clim.*, *28*, 2804-2822.

Marshall, A. G., D. Hudson, M. C. Wheeler, H. H. Hendon, O. Alves (2012), Simulation and prediction of the Southern Annular Mode and its influence on Australian intra-seasonal climate in POAMA, *Clim. Dyn., 38*, 2483-2502.

Marshall, A. G., D. Hudson, H. H. Hendon, M. J. Pook, O. Alves, and M. C. Wheeler (2014), Simulation and prediction of blocking in the Australian region and its influence on intra-seasonal rainfall in POAMA-2, *Clim. Dyn., 42*, 3271-3288.

Marshall, A. G., H. H. Hendon, M. Feng, and A. Schiller (2015), Initiation and amplification of the Ningaloo Niño, *Clim. Dyn., 45*, 2367-2385.

McIntosh P, M. Pook, J. Risbey, P. Hope, G. Wang, and O. Alves (2008), Australia's regional climate drivers, *Tech. Rep.*, Land and Water Australia, Canberra, 48 pp.

McIntosh, P. C., J. S. Risbey, J. N. Brown, and M. J. Pook (2012), Apparent and real sources of rainfall associated with a cutoff low in southeast Australia, *CAWCR Research Letters, 8,* 4-9.

National Climate Centre (2010), A significant rainfall event for central and eastern Australia, Bureau of Meteorology, *Special Climate Statement 20*, 1-8. [http://www.bom.gov.au/climate/current/statements/scs20a.pdf]

Nicholls, N., W. Drosdowsky, and B. Lavery (1997), Australian rainfall variability and change, *Weather, 52*, 66-72.

Raut, B. A., C. Jakob, and M. J. Reeder (2014), Rainfall changes over southwestern Australia and their relationship to the southern annular mode and ENSO, *J. Climate*, *27*, 5801-5814, doi:10.1175/JCLI-D-13-00773.1

Rayner, N. A., D. E. Parker, E. B. Horton, C. K. Folland, L. V. Alexander, D. P. Rowell, E. C. Kent, and A. Kaplan (2003), Global analyses of sea surface temperature, sea ice, and night marine air temperature since the late nineteenth century, *J. Geophys. Res., 108*(D14), 4407, doi:10.1029/2002JD002670.

Risbey, J. S., M. J. Pook, P. C. McIntosh, M. C. Wheeler, and H. H. Hendon (2009), On the Remote Drivers of Rainfall Variability in Australia, *Mon Weather Rev, 137*, 3233-3253.

Saji, N. H., B. N. Goswami, P. N. Vinayachandran, and T. Yamagata (1999), A dipole mode in the tropical Indian Ocean, *Nature, 401*, 360-363.

Slivinski, L. C., G. P. Compo, J. S. Whitaker, P. D. Sardeshmukh, B. S. Giese, C. McColl, R. Allan, X. Yin, R. Vose, H. Titchner, J. Kennedy, L. J. Spencer, L. Ashcroft, S. Brönnimann, M. Brunet, D. Camuffo, R. Cornes, T. A. Cram, R. Crouthamel, F. Domínguez□Castro, J. E. Freeman, J. Gergis, E. Hawkins, P. D. Jones, S. Jourdain, A. Kaplan, H. Kubota, F. Le Blancq, T. Lee, A. Lorrey, J. Luterbacher, M. Maugeri, C. J. Mock, G. K. Moore, R. Przybylak, C. Pudmenzky, C. Reason, V. C. Slonosky, C. Smith, B. Tinz, B. Trewin, M. A. Valente, X. L. Wang, C. Wilkinson, K. Wood, and P. Wyszyński (2019), Towards a more reliable historical reanalysis: Improvements for version 3 of the Twentieth Century Reanalysis system, *Quarterly J. Roy. Meteorol. Soc., 145*, 2876-2908.

Student (1908), The probable error of a mean, *Biometrika, 6*, 1–25.

Taschetto, A. S., and M. H. England (2009), El Niño Modoki Impacts on Australian Rainfall, *J. Clim., 22*, 3167-3174.

Trenberth, K. E. (1979), Interannual variability of the 500 mb zonal-mean flow in the southern hemisphere, *Mon. Wea. Rev., 107*, 1515-1524.

van Rensch, P., A. Gallant, W Cai, and N. Nicholls (2015), Evidence of local sea surface temperatures overriding the southeast Australian rainfall response to the 1997-98 El Niño, *Geophys. Res. Lett., 42*, doi:10.1002/2015GL066319.

van Rensch, P., J. Arblaster, A. J. E. Gallant, W. Cai, N. Nicholls, and P. J. Durack (2019), Mechanisms causing east Australian spring rainfall differences between three strong El Niño events, *Clim. Dyn., 53*, 3641-3659.

Wang, G., and H. H. Hendon (2007), Sensitivity of Australian Rainfall to Inter–El Niño Variations, *J. Clim., 20*, 4211-4226.

Webster, P. J., A. M. Moore, J. P. Loschnigg, and R. R. Leben (1999), Coupled ocean–atmosphere dynamics in the Indian Ocean during 1997–98, *Nature*, *401*, 356-360.

Figure captions

Figure 1. Composites of SST (°C; shading) and OLR (W/m^2; contour) anomalies during the onset phase (April-Sept; left column) and mature phase (Oct-March; right column) for CP El Niño years (n=14; top row) and EP El Niño years (n=8; bottom row). Anomalies are calculated relative to climatology for the period 1900-2015. Stippling indicates statistically significant SST anomalies to 95 % confidence [*Student*, 1908]. Contour interval is 2 W/m^2 with dashed contours representing negative OLR anomalies (enhanced convection), and solid contours representing positive OLR anomalies (reduced convection).

Figure 2. Large panels: Composites of rainfall anomalies (mm) during the onset phase (April-Sept; left column) and mature phase (Oct-March; right column) for CP El Niño years (n=14; top row) and EP El Niño years (n=8; bottom row). Anomalies are calculated relative to climatology for the period 1900-2015. Stippling indicates statistically significant anomalies to 95 % confidence [*Student*, 1908]. Small panels: significant rainfall anomalies for three-month rolling seasons through the composite lifecycle of CP (top row) and EP (bottom row) El Niño events.

Figure 3. Pearson correlation coefficients of Australian rainfall anomalies with the Niño-4 index during the onset phase (April-Sept; left column) and mature phase (Oct-March; right column) for CP El Niño years (n=14; top row) and EP El Niño years (n=8; bottom row). Stippling indicates statistically significant SST anomalies to 95 % confidence [*Student*, 1908]. The upper panels show the southeast Australian / Murray Darling Basin box region (dotted lines; refer to the text for

details), and a scatter plot of area-averaged rainfall anomalies in box region versus Niño-4 index values during the onset phase (top left) and mature phase (top right) of CP events.

Figure 4. (a) Pearson and Spearman correlation coefficients of southeast Australian / Murray Darling Basin rainfall anomalies with the Niño-4 index for three-month rolling seasons through the composite lifecycle of CP El Niño events. (b) Rainfall anomalies in the southeast Australian / Murray Darling Basin region for three-month rolling seasons through the composite lifecycle of the strongest (red) and weakest (blue) three (solid bold), five (solid) and seven (dash-dot) CP El Niño events. The grey line emphasises the strong CP event of 2019-2020 (also included in the composite for the strongest seven events). (c)-(f) Composite of anomalous mean sea level pressure (Pa; shading) and 850 hPa horizontal wind (m s^{-1}; vector arrow) for the strongest seven (top row) and weakest seven (bottom row) CP events, calculated as the difference from the CP event climatology, for August – October (ASO; left column) and January – March (JFM(+); right column).

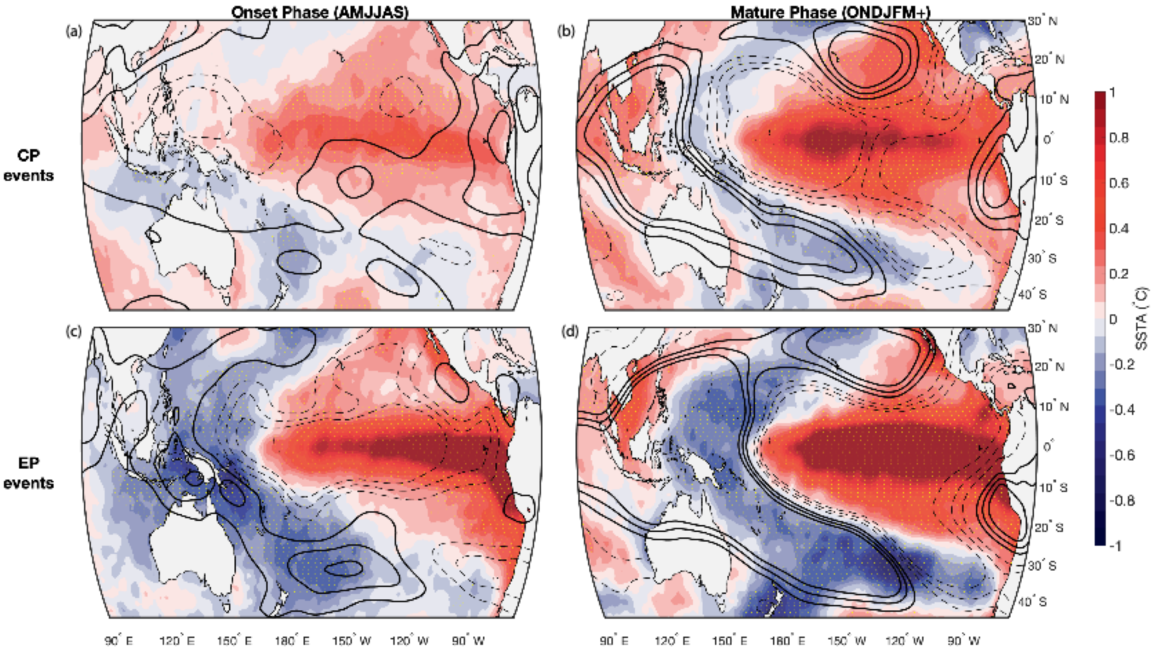
Onset Phase (AMJJAS)
Mature Phase (ONDJFM+)
(a)
(b)
(c)
(d)
CP events
EP events
30° N
20° N
10° N
0°
10° S
20° S
30° S
40° S
90° E
120° E
150° E
180° E
150° W
120° W
90° W
SSTA (°C)
1
0.8
0.6
0.4
0.2
0
-0.2
-0.4
-0.6
-0.8
-1

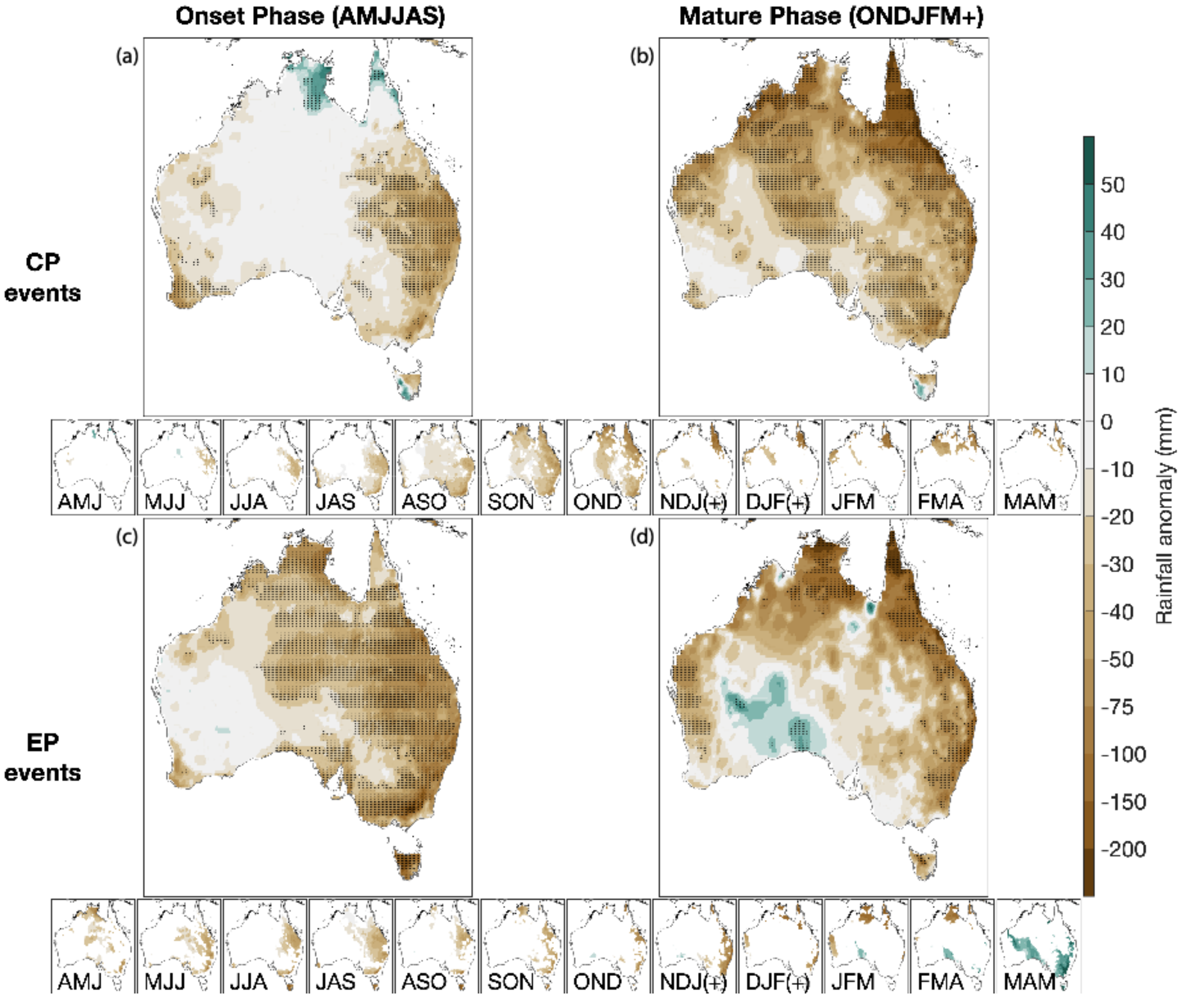
Onset Phase (AMJJAS)
Mature Phase (ONDJFM+)
(a)
(b)
(c)
(d)
CP
events
EP
events
AMJ
MJJ
JJA
JAS
ASO
SON
OND
NDJ(+)
DJF(+)
JFM
FMA
MAM
50
40
30
20
10
0
-10
-20
-30
-40
-50
-75
-100
-150
-200
Rainfall anomaly (mm)

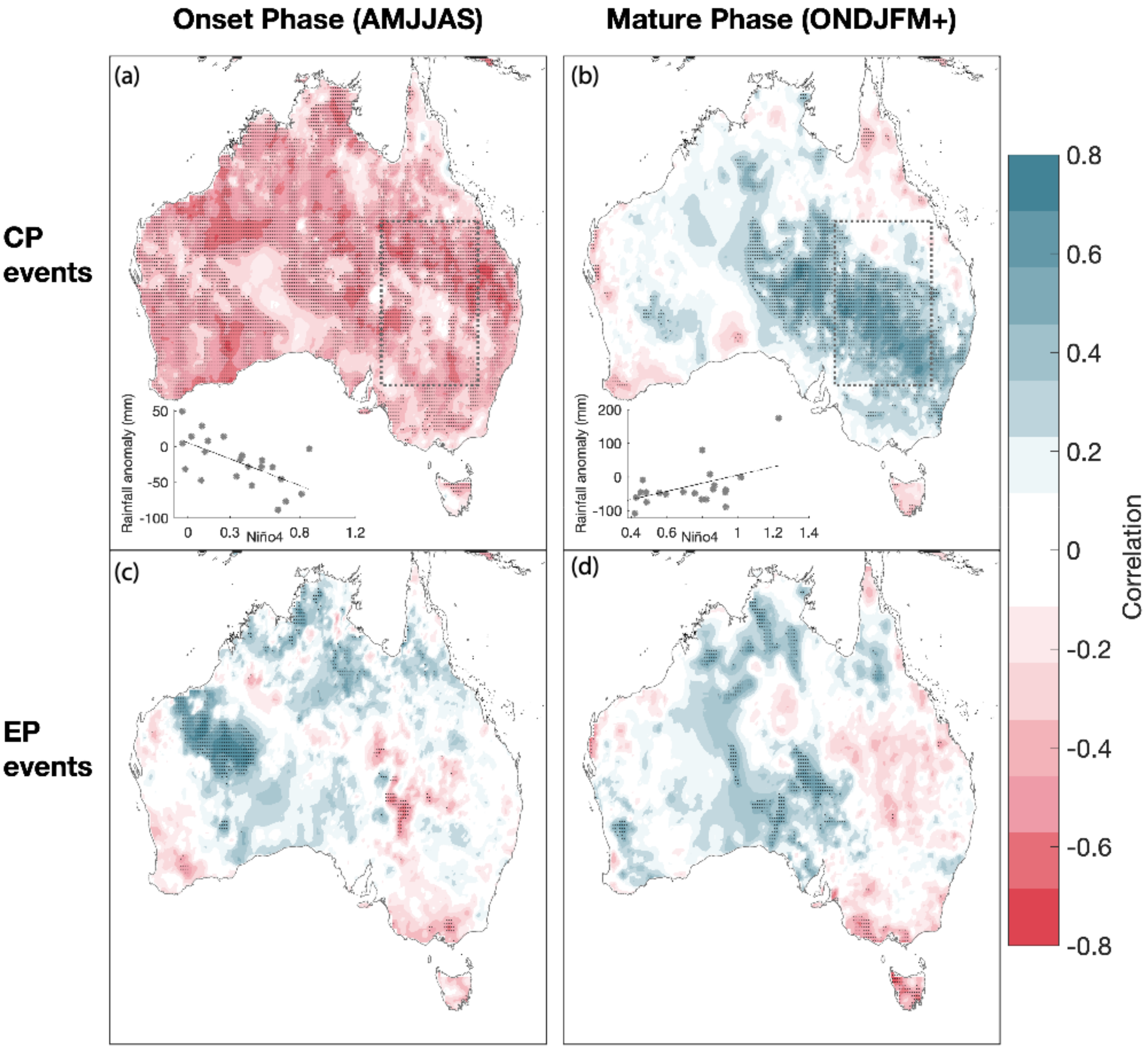
Onset Phase (AMJJAS)
Mature Phase (ONDJFM+)
CP events
EP events
(a)
(b)
(c)
(d)
Rainfall anomaly (mm)
Niño4
Correlation
0.8
0.6
0.4
0.2
0
-0.2
-0.4
-0.6
-0.8

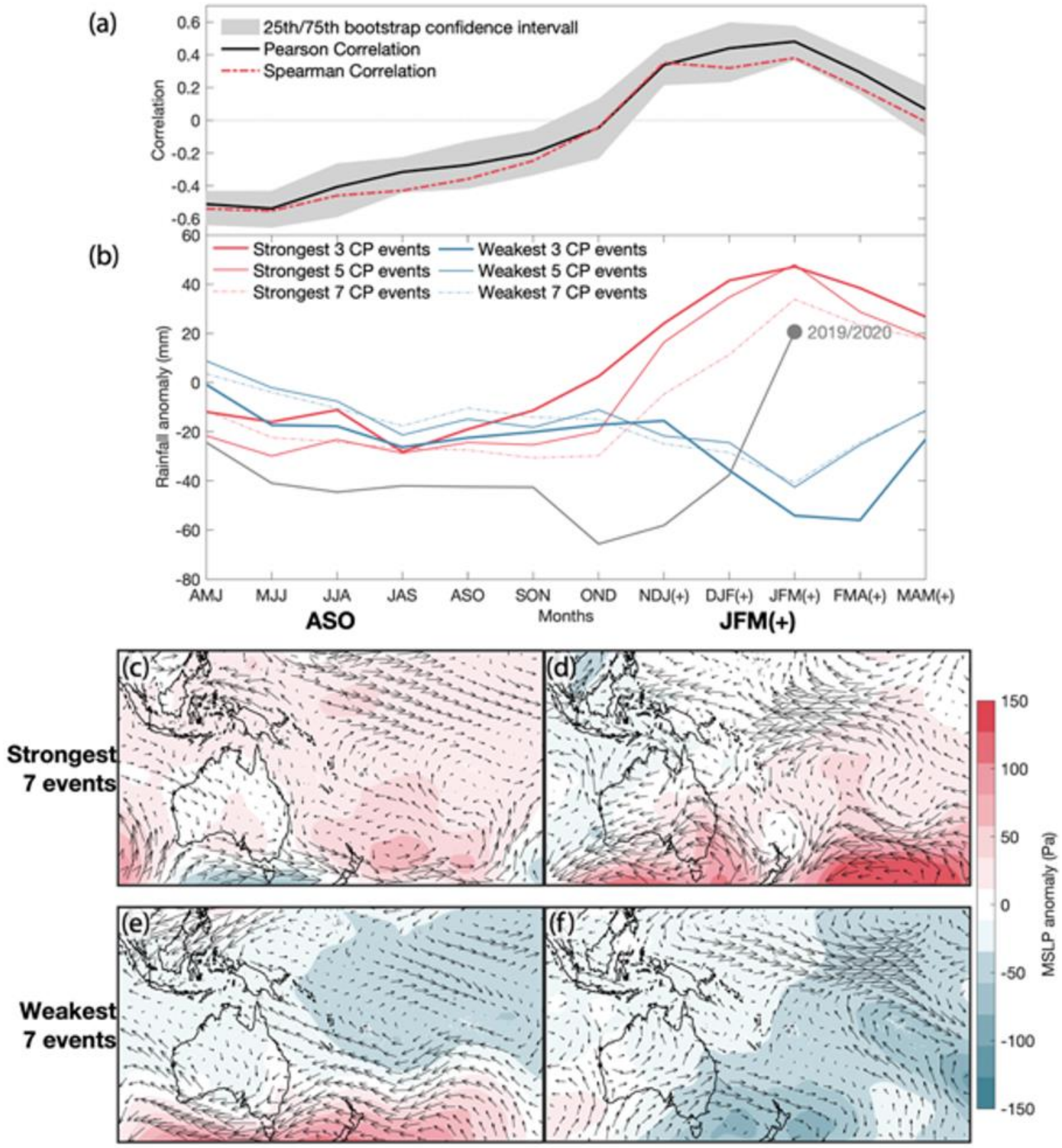
(a)
25th/75th bootstrap confidence intervall
Pearson Correlation
Spearman Correlation
Correlation
0.6
0.4
0.2
0
-0.2
-0.4
-0.6
(b)
Strongest 3 CP events
Strongest 5 CP events
Strongest 7 CP events
Weakest 3 CP events
Weakest 5 CP events
Weakest 7 CP events
2019/2020
Rainfall anomaly (mm)
60
40
20
0
-20
-40
-60
-80
AMJ
MJJ
JJA
JAS
ASO
SON
OND
NDJ(+)
DJF(+)
JFM(+)
FMA(+)
MAM(+)
Months
ASO
JFM(+)
(c)
(d)
Strongest 7 events
(e)
(f)
Weakest 7 events
MSLP anomaly (Pa)
150
100
50
0
-50
-100
-150